



SHAKING TABLE TEST OF RC BOX-TYPE SHEAR WALL IN MULTI-AXES LOADING

Haruhiko TORITA¹, Ryoichiro MATSUMOTO², Yoshio KITADA³,
Kazuhiro KUSAMA⁴, Takao NISHIKAWA⁵

SUMMARY

Shaking table test has been conducted as a part of a test project, 'Model Test of Multi-axes Loading on RC (reinforce concrete) Shear Walls' aiming at verifying the strength and restoring force characteristics of RC shear walls. Most of the project had been performed by Nuclear Power Engineering Corporation (NUPEC), which was succeeded recently by Japan Nuclear Energy Safety Organization (JNES).

Two box-type shear wall specimens were tested to check the reproducibility of the test results. The dimension of the specimen is 1.5m square in plan, 1m in height and 75mm in thickness. The rebars used for walls are 6mm in diameter and their arrangement is double at the spacing of 70mm in both vertical and horizontal directions. The reinforcement ratio, pw, is 1.2%. We have used normal pea gravel concrete, whose design strength was about 35MPa. A specimen of a cylindrical wall was also tested to be compared to the test results of box-type specimens.

Dynamic loading test was planned to study the fundamental response properties of the specimens in wide range of dynamic responses from elastic region to plastic ultimate state under multi directional loading. We made three independent components of input motion to fit a target response spectrum which is flat from 0.04sec to 0.2sec. The acceleration level of vertical component was set as half of those in the horizontal directions. Six steps of excitation were planned to increase acceleration level step-by-step, from Run-1 for elastic response to Run-6 for ultimate loading step. In this paper we summarize the results of dynamic tests focusing on ratios of deformation components, applicability of skeleton curve of restoring force characteristics derived from results of one directional loading test, and equivalent viscous damping factors.

INTRODUCTION

¹ Shimizu Corporation, Tokyo, JAPAN, Email:tori@shimz.co.jp

² Shimizu Corporation, Tokyo, JAPAN, Email:matsuromotor@shimz.co.jp

³ Japan Nuclear Energy Safety Organization, Tokyo, JAPAN, Email:kitada-yoshio@jnes.go.jp

⁴ Japan Nuclear Energy Safety Organization, Tokyo, JAPAN, Email:kusama-kazuhiro@jnes.go.jp

⁵ Tokyo Metropolitan University, Tokyo, JAPAN, Email:tanishi@arch.metro-u.ac.jp

An earthquake strikes a Nuclear Power Plant (NPP) building in three directions simultaneously. Nevertheless there are little data to study a three-dimensional behavior of RC structures in NPPs up to their ultimate states by applying three directional dynamic loads. Considering the situations, NUPEC had started the test project, 'Model Test of Multi-axes Loading on RC Shear Walls' under the commission of Ministry of Economy, Trade and Industry of Japan (METI). JNES succeeded to the project since October 2003. The dynamic loading test was conducted as a part of the project, using a shaking table of Public Works Research Institute in Japan. Authors suppose that it is one of the first attempts in the world to test RC shear walls up to their ultimate state under the multi-directional dynamic loading. In this paper we describe an outline of the dynamic loading test program and summarize the test results. Also we discuss some topics regarding response characteristics of RC specimens, such as deformation components ratios, an applicability of skeleton curve of restoring force characteristics obtained in one directional loading test and equivalent viscous damping factors.

OUTLINE OF TEST PROGRAM

Specimen

A specimen consists of three parts; shear walls, a base slab, and an upper slab. Dimensions of the walls of box-type specimens are 1.5m square x 1m height x 75mm thickness. Rebar arrangement for the walls is 2-D6@70 in both vertical and horizontal directions, to make reinforcement ratio $\rho_w=1.2\%$. In case of the cylindrical-type specimen, the diameter of center line of the wall is 1.91m. Height, thickness, cross sectional area, and reinforcement ratio of the cylindrical wall were set to be equal to those of box-type specimens. Two box-type specimen DT-B-01 and DT-B-02, and a cylindrical-type specimen DT-C-01 were made. Shape and rebar arrangement of specimens are shown in Fig.1-Fig.3. The walls were made of normal concrete with pea gravel. Material properties are in Table1.

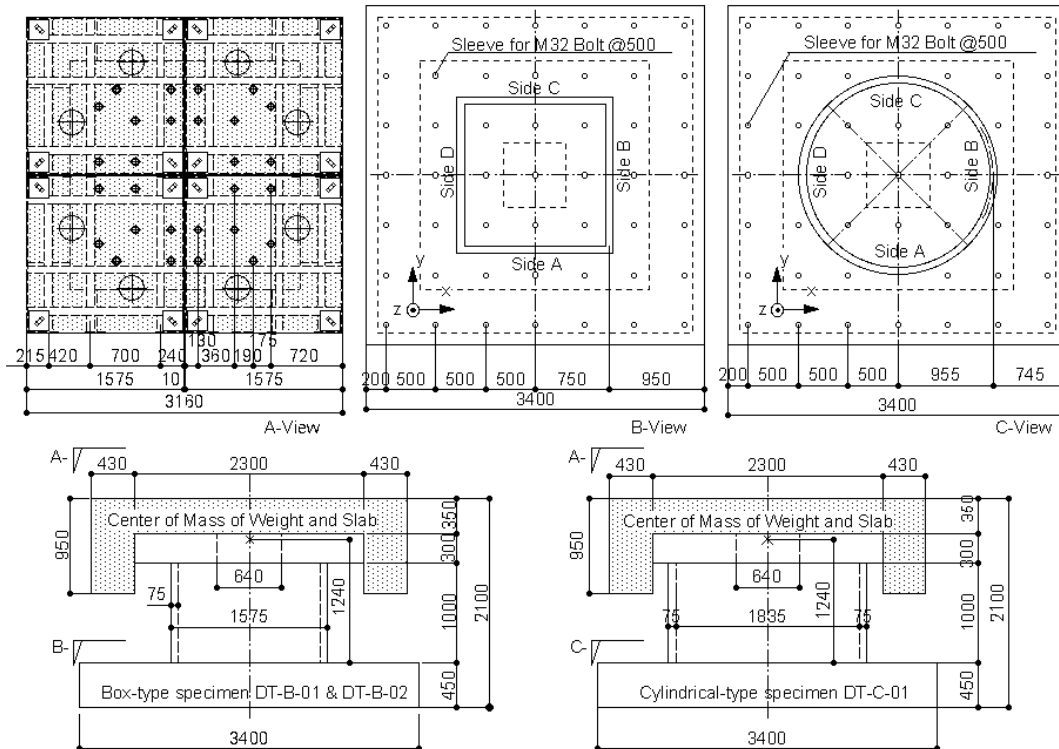
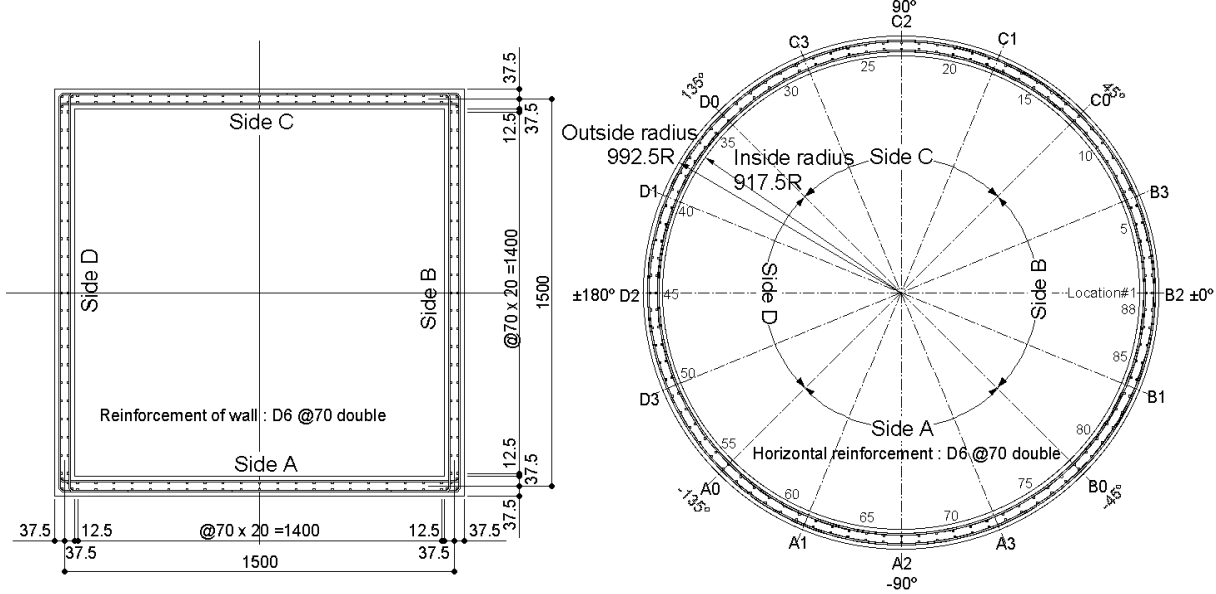


Fig.1 Shape of specimen (unit:mm)



(a) Box-type DT-B-01 and DT-B-02 specimen (b) Cylindrical type DT-C-01 specimen
Fig.2 Rebar arrangement of specimen (unit:mm)

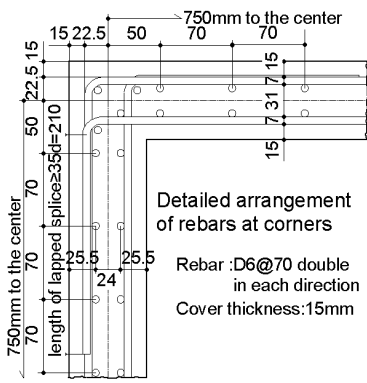


Fig.3 Detail at corners of box-type specimen (unit:mm)

Table1 Material properties

Mix proportion of concrete	DT-B-01	DT-B-02	DT-C-01
Water cement ratio (%)	65.0	67.0	62.0
Sand aggregate ratio (%)	52.0	54.0	52.5
Unit water content (kg/m ³)	178	180	172
Cement (kg/m ³)	274	269	277
Sand (kg/m ³)	951	969	938
Pea gravel (kg/m ³)	840	822	848
Pozolite#70 (kg/m ³)	0.685	0.673	2.77

Concrete property	DT-B-01	DT-B-02	DT-C-01
Comp. strength σ_B (MPa)	38.6	34.4	37.5
Comp. strain ϵ_0 at σ_B (μ)	-2033	-2207	-1928
Young's modulus E_c (GPa)	29.3	26.6	30.7
Poisson's ratio ν_c	0.20	0.19	0.16
Split tensile strength (MPa)	2.63	2.88	3.00
σ_B of upper slab (MPa)	46.8	40.5	46.7
σ_B of base slab (MPa)	39.7	43.6	48.3

Four blocks of weights, each of which weighed 15.62ton, were attached on the upper slab with PC rods, to make axial stress at the bottom of the walls due to dead load 1.47MPa. Taking weight blocks, an upper slab, and an upper half of walls as a lumped mass point, total mass was 67ton and values of rotational inertia were $I_x=I_y=71.7\text{ton}\cdot\text{m}^2$ and $I_z=112\text{ton}\cdot\text{m}^2$.

Excitation plan

Three components of artificial input motions, duration of which were 7 seconds, were made from uniform random numbers. The level of vertical acceleration in target response spectra is set half of those in horizontal directions. Six input steps of excitation shown in Fig.4 were set in the original excitation plan, so that sufficient response data to clarify dynamic response characteristics of the specimens can be obtained. These steps were executed from Run-1 to Run-6 with increasing input acceleration levels. Acceleration response spectra and acceleration time history of input motions are shown in Fig.5 and Fig.6.

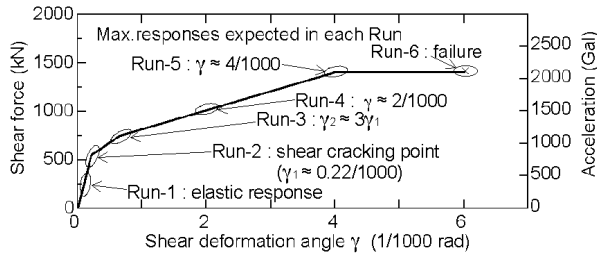


Fig.4 Max. resp. expected in each Run

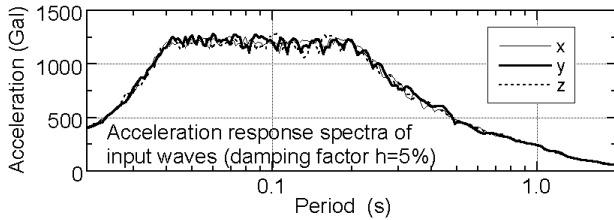


Fig.5 Response spectra of input waves

Measurement plan

Measurement plan was made assuming that the upper slab and the base slab approximately behave like rigid bodies. Acceleration, displacement, strain of vertical wall reinforcement were measured. Arrangement of sensors for measuring displacement and acceleration are shown in Fig.7. Sampling period in data acquisition was 400Hz for DT-B-01 and Run-1&2 of DT-B-02, and 1000Hz for the rest. Low-pass filter, whose characteristics is shown in Fig.8, were applied to the acquired data.

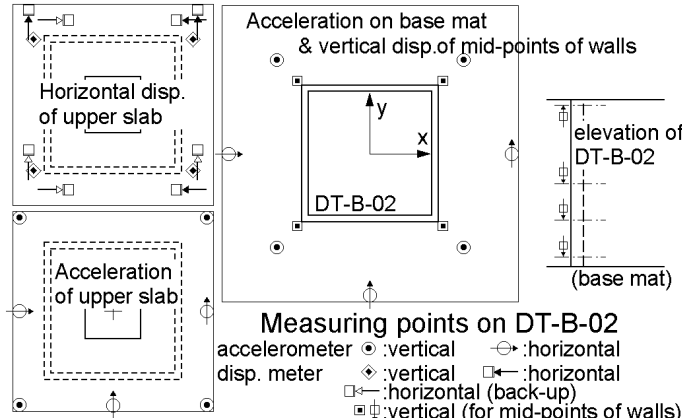


Fig.7 Measuring points on DT-B-02 specimen

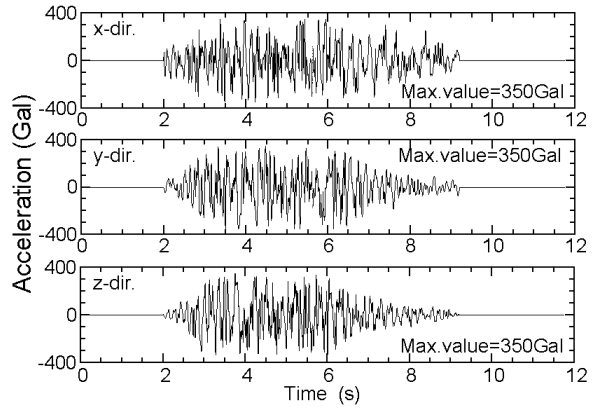


Fig.6 Time history of input waves

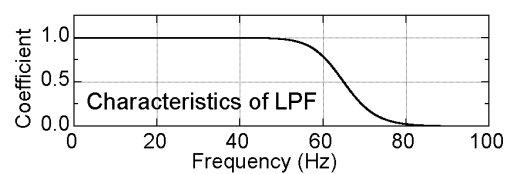


Fig.8 Characteristics of L.P.F.

TEST RESULTS

Crack patterns

Crack patterns in DT-B-02 specimen are shown in Fig.9. Bending cracks were observed at the foot of the walls after Run-1. Initial shear cracks were found at the mid portion of the wall after the excitation step of Run-2, in which initiation of shear crack was expected. The number of cracks in the wall gradually increases after Run-2. In the final excitation step, concrete at the foot of the walls fell down totally.

Also shown in Fig.10 are crack patterns observed in DT-C-01 test. Because of four safety protection steel columns set close to the cylindrical wall, intensive crack observation at 0° , 90° , $\pm 180^\circ$, and -90° was

difficult until these columns were removed. Initial bending cracks were found after Run-2' and the first shear cracks were found after Run-3 in this case. Though the crack patterns at failure looks similar to those of DT-B-02, most of shear cracks formed at the mid-height of the cylindrical wall before failure.

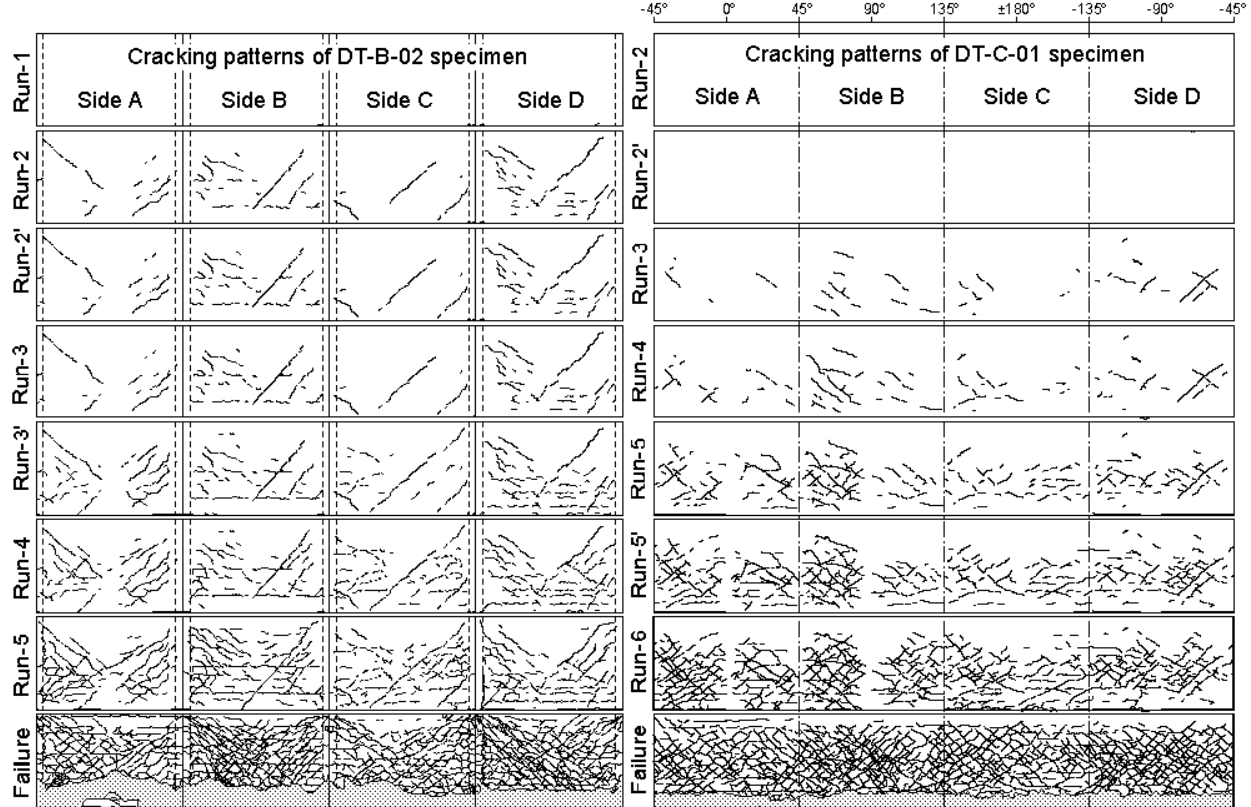


Fig.9 Crack patterns of DT-B-02 specimen

Fig.10 Crack patterns of DT-C-01 specimen

Acceleration time history and hysteresis curve of response

Time history waves of horizontal response acceleration of the upper slab are shown in Fig.11. Upper half of the figure are graphs of DT-B-02 and lower half are those of DT-C-01. Hysteresis response curve regarding displacement and acceleration of DT-B-02 are shown in Figs.12 and Fig.13. Acceleration-displacement relationship curves of Fig.12 show that the slip nature of reverse-S shape in the graphs getting clearer as the excitation steps goes on. The second graph of Fig.13 shows a horizontal displacement-vertical displacement relationship curve. The curve shows shape like a shallow bowl. Residual vertical displacement shown in the graph means increase of bending cracks left unclosed.

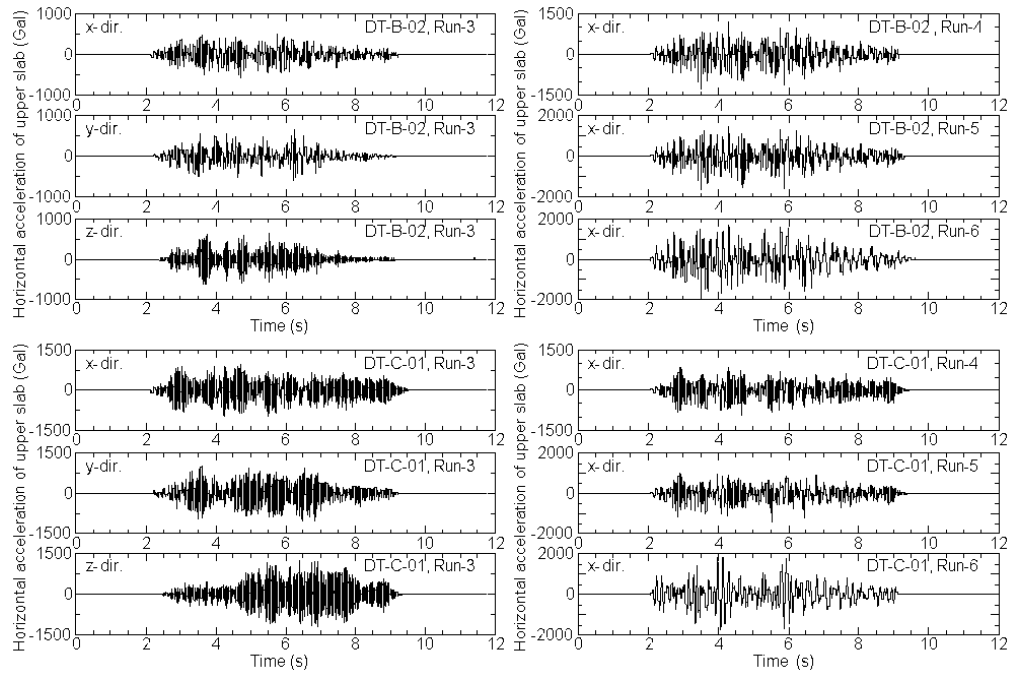


Fig.11 Time history of horizontal acceleration waves

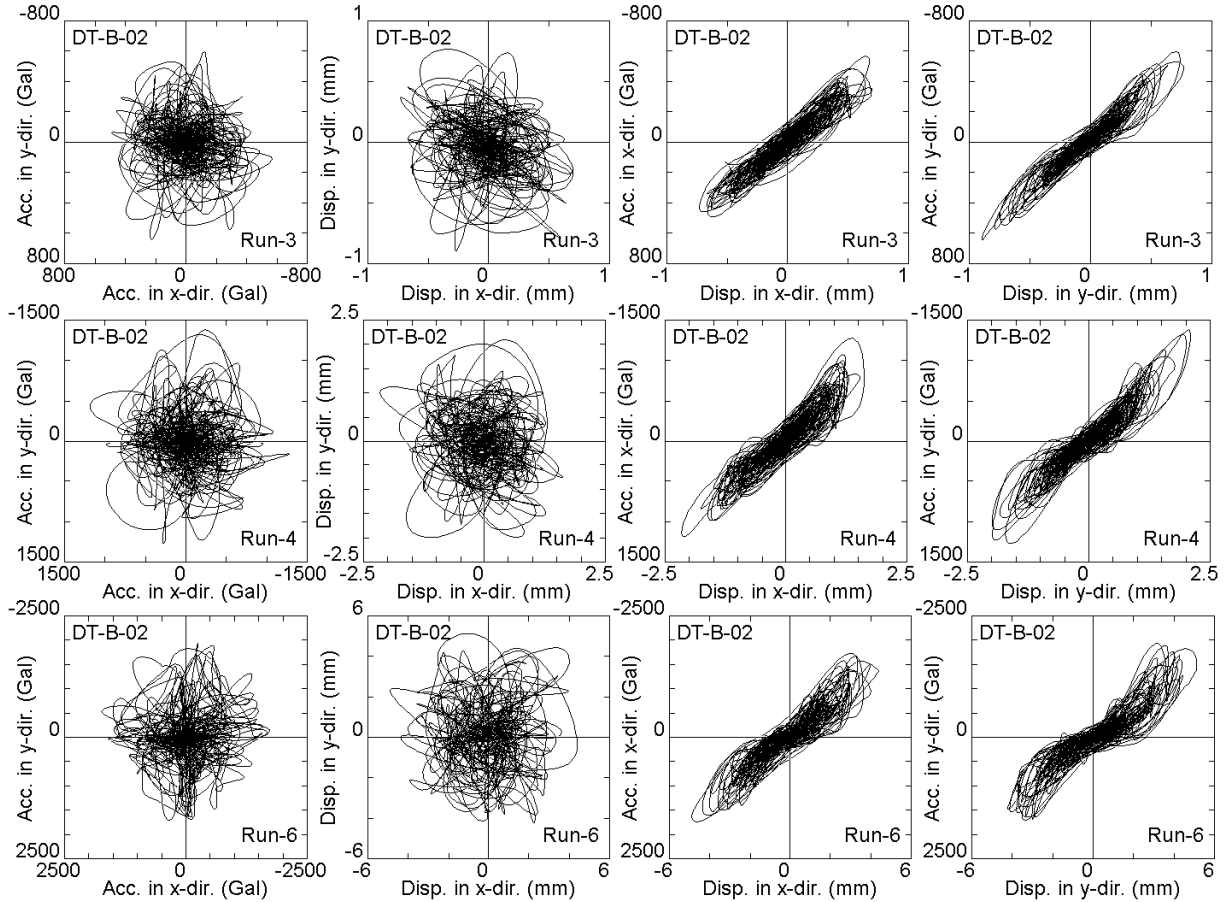


Fig.12 Hysteresis loop of horizontal response

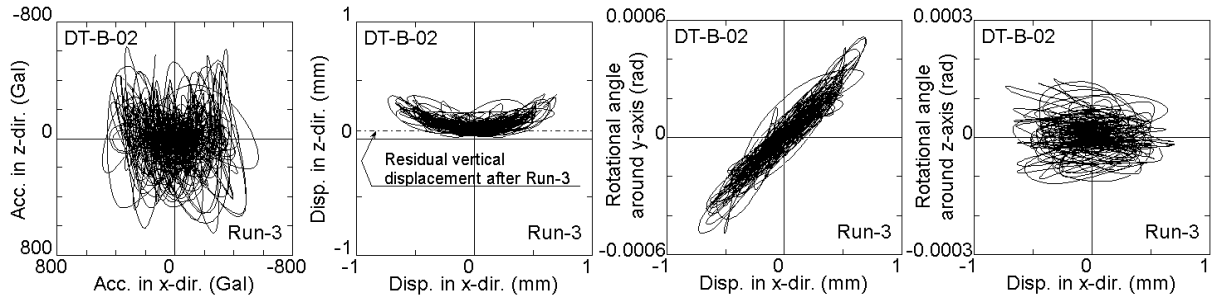


Fig.13 Hysteresis loop of horizontal response and other quantities

Changes of response characteristics

Change of natural frequency f_1 of the specimens are summarized in Table2 and Fig.14.

Initial natural frequencies in horizontal directions were 22-23Hz in DT-B-01, 20-21Hz in DT-B-02, and 24Hz in DT-C-01. These values fell down remarkably after experience of early steps of excitation to become 6-8Hz just before failure.

Table2 Natural frequencies f_1 measured before each Run (unit:Hz)

DT-B-01	x-dir.	y-dir.	z-dir.	DT-B-02	x-dir.	y-dir.	z-dir.	DT-C-01	x-dir.	y-dir.	z-dir.
Run-0	22.5	22.5	46.8	Run-1	20.6	20.4	42.8	Run-1	24.1	24.1	47.1
Run-1	15.2	14.4	36.4	Run-2	20.3	22.3	44.5	Run-2	23.7	23.6	45.5
Run-2	16.2	15.1	34.6	Run-2'	15.4	13.8	39.2	Run-2'	23.4	23.2	45.1
Run-3	13.1	14.2	33.4	Run-3	15.2	13.6	39.6	Run-3	22.9	21.9	44.4
Run-3'	11.5	13.1	33.0	Run-3'	14.8	13.4	39.5	Run-4	21.5	20.4	42.3
Run-4	12.0	12.5	30.6	Run-4	14.5	13.0	39.5	Run-5	21.0	20.2	42.5
Run-5	12.5	11.8	33.8	Run-5	14.3	12.2	38.1	Run-5'	18.7	18.1	39.7
Run-6	8.8	7.2	29.9	Run-6	13.0	11.5	37.9	Run-6	9.2	9.5	34.5
f_1 before each Run (Hz)				Run-7	7.3	6.4	32.4	Run-7	7.6	7.5	33.0

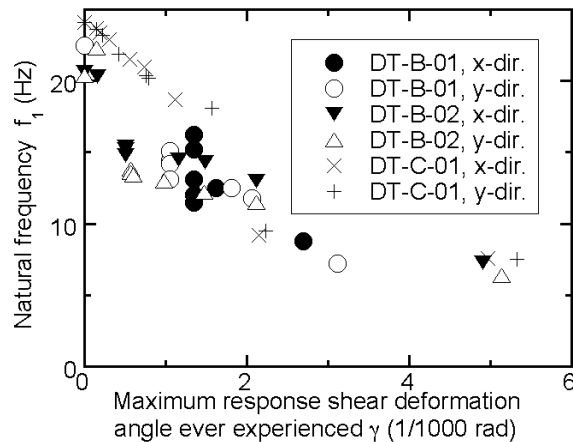
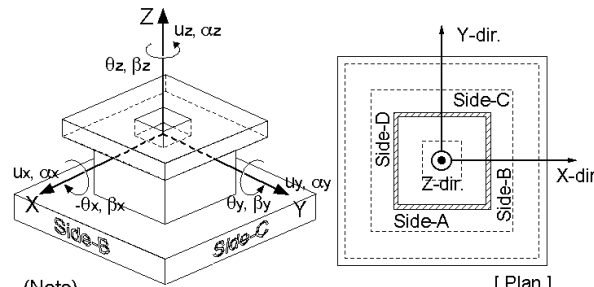


Fig.14 γ - f_1 relationship

If a target response level could not be attained, another excitation step was added. That is the reason why Run numbers of the tests differ from the original excitation plan shown in Fig.4. Some of maximum response values in each step are shown in Table3. Cross sectional forces listed at the bottom of the table are inertia forces derived from acceleration. Shear deformation angle γ and flexural component of deformation u_b are derived in the manner described in the next sub-section.

Table3 Maximum response values in each excitation step

DT-B-01	Run-0	Run-1	Run-2	Run-3	Run-3'	Run-4	Run-5	Run-6	DT-B-02	Run-1	Run-2	Run-2'	Run-3	Run-3'	Run-4	Run-5	Run-6	Run-7
Cxbase [Gal]	-1512	-165	384	460	-735	-1162	-1617	-1678	Cxbase [Gal]	143	933	256	484	1063	1005	1499	-1950	-1551
Cybase [Gal]	-554	-148	-514	751	-910	-1186	-1570	-1754	Cybase [Gal]	-122	-826	-173	340	-731	982	-1231	-2131	-1893
Czbase [Gal]	1537	-105	321	515	721	996	-985	635	Czbase [Gal]	85	839	181	375	777	712	1050	1385	941
Bxbase [rad/s ²]	-2.32	-0.55	1.82	2.29	-2.72	2.50	2.80	-1.89	Bxbase [rad/s ²]	-0.45	-2.60	-0.52	1.22	2.47	3.01	3.92	4.59	-2.75
Bybase [rad/s ²]	-10.76	-0.67	-2.18	2.46	-4.29	-5.84	7.14	-7.65	Bybase [rad/s ²]	-0.50	3.25	-0.76	1.44	-4.22	3.69	6.47	8.04	1.87
Bzbase [rad/s ²]	2.10	0.08	-0.25	-0.35	0.55	0.59	1.03	0.91	Bzbase [rad/s ²]	-0.10	0.53	0.18	-0.22	0.52	0.57	0.77	-1.17	-0.79
Cxtop [Gal]	-1231	268	-620	-846	989	-1489	-1955	1604	Cxtop [Gal]	-472	-941	-359	-568	-1113	-1275	-1649	1739	-1780
Cytop [Gal]	650	-259	-754	967	1450	-1707	2115	-2235	Cytop [Gal]	433	-766	335	642	-1153	-1383	-1794	-1934	-2672
Cztop [Gal]	-2497	250	-669	969	1350	1726	1905	1490	Cztop [Gal]	-182	1152	285	650	-1786	-1395	2105	2190	1435
Bxtop [rad/s ²]	-7.37	-1.82	8.86	10.41	14.30	14.53	16.77	-17.63	Bxtop [rad/s ²]	-2.99	-7.97	-1.70	4.22	8.62	-11.75	12.71	18.78	16.80
Bytop [rad/s ²]	-19.54	2.15	5.25	-6.55	-9.82	12.19	-16.04	13.98	Bytop [rad/s ²]	3.45	9.66	3.68	-5.64	-12.13	-12.15	-15.19	17.03	-14.76
Bztop [rad/s ²]	5.56	0.44	1.48	-1.93	-3.01	3.27	5.08	4.02	Bztop [rad/s ²]	-0.30	1.79	0.55	1.50	-2.80	-2.63	4.07	-4.65	5.54
Ux [mm]	1.520	0.351	0.767	1.209	1.863	2.704	4.288	8.942	Ux [mm]	0.260	-0.938	-0.471	-0.733	-1.779	-2.160	-3.004	-4.901	18.941
Uy [mm]	-0.443	-0.259	0.858	-1.383	-2.499	-2.765	-4.246	15.855	Uy [mm]	-0.230	-1.011	-0.459	-0.893	1.419	2.097	3.005	5.135	-26.349
Uz [mm]	1.049	0.240	0.420	0.724	4.121	1.248	1.894	3.712	Uz [mm]	0.018	0.620	0.200	0.385	0.814	0.925	1.297	-	-
-ox [0.001 rad]	-0.435	0.122	0.749	0.929	3.502	1.540	1.964	4.131	-ox [0.001 rad]	-0.109	-0.673	0.179	0.471	0.843	-1.036	-1.272	-	-
oy [0.001 rad]	-1.544	0.225	0.488	0.677	-4.070	1.759	2.644	-2.140	oy [0.001 rad]	-0.138	-0.909	-0.280	0.516	-1.087	1.126	1.805	-	-
oz [0.001 rad]	-0.071	-0.056	-0.171	0.327	-0.554	0.804	-1.156	4.003	oz [0.001 rad]	-0.024	0.187	0.084	0.150	0.370	-0.524	0.610	1.548	10.786
γ_x [0.001 rad]	1.345	-0.218	0.472	0.712	-1.097	1.620	2.698	6.764	γ_x [0.001 rad]	0.156	-0.508	-0.312	-0.447	-1.155	-1.482	-2.114	-4.901	18.941
γ_y [0.001 rad]	1.056	-0.181	-0.501	-0.845	-1.815	-2.067	-3.118	12.054	γ_y [0.001 rad]	-0.151	-0.571	-0.350	-0.603	0.975	1.473	2.120	5.135	-26.349
Ubx [mm]	0.542	0.084	0.188	0.272	0.499	0.683	-0.646	-0.652	Ubx [mm]	-0.028	-0.432	-0.177	-0.297	-0.537	-0.554	-0.784	-	-
Uby [mm]	-0.737	0.059	0.290	0.368	0.557	0.655	0.713	0.749	Uby [mm]	-0.022	0.295	-0.104	-0.200	-0.367	-0.482	-0.631	-	-
Ox [kN]	824	-179	415	567	-662	997	1309	-1074	Ox [kN]	316	630	241	380	745	854	1104	-1165	1192
Oy [kN]	-436	174	505	-647	-971	1144	-1416	1496	Oy [kN]	-290	513	-224	-430	772	926	1202	1296	1790
Nz [kN]	2213	825	1052	1306	1561	1814	1933	1656	Nz [kN]	757	1429	848	1092	1836	1588	2067	2125	1619
Tz [kN m]	-622	-49	-166	216	338	-366	-570	-451	Tz [kN m]	34	-200	-62	-168	314	295	-456	521	-621



(Note)

- α,β :sway and rotational acceleration,
- u,θ :sway and rotational displacement,
- γ :shear deformation angle,
- ub :flexural component of horizontal displacement,
- Q,N,T :shear force, axial force, and torque around vertical axis,
- base,top :suffix to distinguish the base slab and the upper slab
- Max.values before failure are adopted for the last Runs.

DT-C-01	Run-1	Run-2	Run-2'	Run-3	Run-4	Run-5	Run-5'	Run-6	Run-7
Cxbase [Gal]	115	199	346	868	794	1311	1566	-1212	-1466
Cybase [Gal]	-126	-190	429	938	891	-1525	-1724	-1327	-1680
Czbase [Gal]	110	145	225	907	-699	847	-1071	-752	918
Bxbase [rad/s ²]	-0.57	-0.85	0.60	2.67	2.89	-4.55	4.33	1.63	2.11
Bybase [rad/s ²]	-0.63	-0.81	-0.82	-2.36	2.68	-4.07	5.59	-1.30	-2.23
Bzbase [rad/s ²]	0.12	-0.16	-0.25	0.55	-0.41	0.68	-0.80	-0.60	39.58
Cxtop [Gal]	516	595	-857	-974	-907	-1397	-1474	1844	-1631
Cytop [Gal]	523	678	-1140	-1013	-920	-1358	-1712	-1935	-1825
Cztop [Gal]	208	325	447	1251	1116	-1341	1905	1698	1415
Bxtop [rad/s ²]	-3.10	-4.61	-6.16	-7.56	7.56	-13.26	-13.10	12.57	-7.98
Bytop [rad/s ²]	-3.17	-3.83	-5.62	-7.23	-7.84	-13.97	-10.27	-10.12	-10.29
Bztop [rad/s ²]	-0.36	-0.51	-1.12	-3.05	-2.23	3.59	4.64	3.98	-3.22
Ux [mm]	-0.228	-0.304	0.485	1.030	-1.132	-1.716	-3.028	-6.388	8.296
Uy [mm]	-0.236	0.349	0.681	-1.205	-1.237	-2.157	-2.912	-6.845	8.863
Uz [mm]	0.022	0.036	0.123	0.600	0.593	0.888	1.244	1.868	-
-ox [0.001 rad]	0.122	0.187	0.291	0.571	-0.557	1.005	1.246	1.530	-
oy [0.001 rad]	-0.122	0.143	0.273	0.559	-0.636	0.983	-0.903	-1.709	-
oz [0.001 rad]	0.023	-0.025	0.072	0.246	0.244	-0.719	-1.000	-1.306	3.163
γ_x [0.001 rad]	-0.143	-0.189	-0.306	0.558	-0.734	1.112	-2.150	-4.966	8.328
γ_y [0.001 rad]	-0.149	0.220	0.421	0.764	-0.785	-1.571	2.236	-5.332	8.951
Ubx [mm]	0.005	-0.011	0.036	0.205	0.228	0.415	0.448	-1.084	-
Uby [mm]	-0.011	-0.021	-0.044	-0.210	-0.205	-0.388	-0.502	0.989	-
Ox [kN]	-346	-399	574	652	607	936	988	-1235	1093
Oy [kN]	-350	-454	763	678	616	910	1147	1296	1222
Nz [kN]	796	875	957	1495	1405	1497	1933	1794	1605
Tz [kN m]	41	57	125	341	250	-402	-520	-446	361

Deformation component ratios

Horizontal displacement of the upper slab contains not only flexural and shear deformation of the walls, but also displacement caused by rotation. Though D6 is the smallest size deformed bar available, bar diameter is relatively big compared to the size of the walls. It is also true that ribs on the surface of the bar is quite small compared to aggregate size. So it is expected that flexural cracks formed at boundaries between the walls and the slabs tend to open relatively wide, to cause rotation of the walls and the upper slab.

Rotations at z=0-60mm and z=970-1000mm, where z is a height from the surface of the base slab, are calculated from data of vertical displacement meters. Flexural deflection curve of the walls can be estimated from rotations at z=60,280,500 and 970mm, as is shown in Fig.15. Subtracting displacement due to rotation and flexural deformation from the total horizontal displacement yields shear deformation.

Thus every horizontal displacement data can be decomposed into four components; flexural deformation, shear deformation, deformation at the top part of the walls, and deformation at the bottom part of the walls

including displacement due to rotation. Ratios of four components to the total displacement at every moment are averaged in the manner shown in Fig.16.

Transition of the ratios as excitation steps go on in case of DT-B-02 specimen are shown in Fig.17 as an example. The ratio of the bottom part was pretty high in Run-1, as cracks formed only at boundaries between the walls and the base slab. It dropped after Run-2, as shear and flexural cracks appeared. After Run-2, ratios of four components did not change so much until failure.

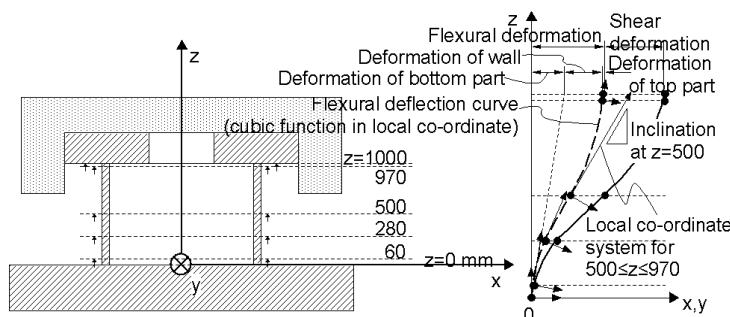


Fig.15 Decomposition of deformation component

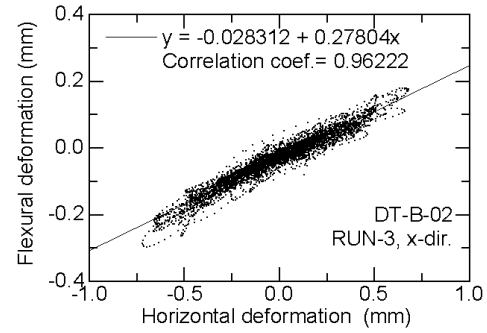


Fig.16 Linear regression to derive flexural component ratio

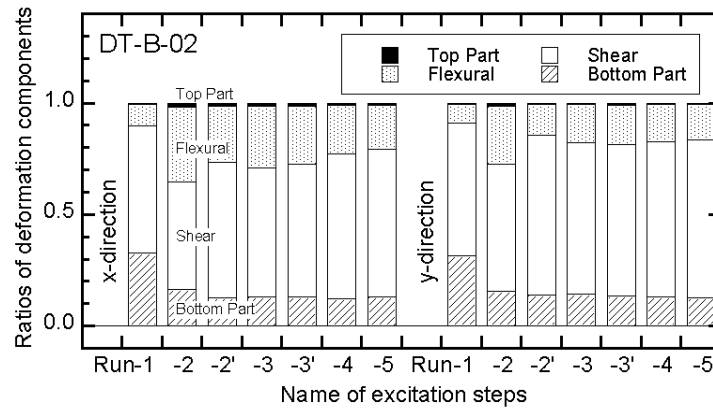


Fig.17 Transition of ratios of deformation components

Comparison of maximum response values and skeleton curves for uni-axial loading

Resultant shear force Q calculated from Q_x and Q_y are checked if the maximum value is renewed. Renewal points, at which the maximum value of resultant Q from the beginning of the first Run to the current time was renewed, are plotted against resultant shear deformation angles in Fig.18. Renewal points in each excitation step are plotted too, with using small dots.

Also plotted are examples of skeleton curves for uni-axial loading evaluated by equations in JEAG 4601 [1,2], which is a technical guidelines for seismic design of nuclear power plant in Japan. It is confirmed by Ono et al.[3] that a skeleton curve of $Q-\gamma$ relationship under varying axial force ranges between upper and lower bound curves; a skeleton curve under the maximum axial force and a skeleton curve under the minimum axial force. So three skeleton curves for three constant values of axial compressive stress of the walls $\sigma_v=1.47, 2.94, 0.0$ MPa are plotted to take effects of varying axial force into account. These values of axial stress correspond to vertical response acceleration 0G, +1G, and -1G respectively.

Comparing test results to evaluated curves for uni-axial loading, the latter can be used as the first order approximation to the former, if used in the region where nonlinearity is weak. In case of DT-C-01 specimen, a plot point of Run-6 seems to be slightly softer than the evaluated curves. As slip between the wall and the base slab became dominant in Run-7, evaluated shear deformation angle of the point may contain component of the slip.

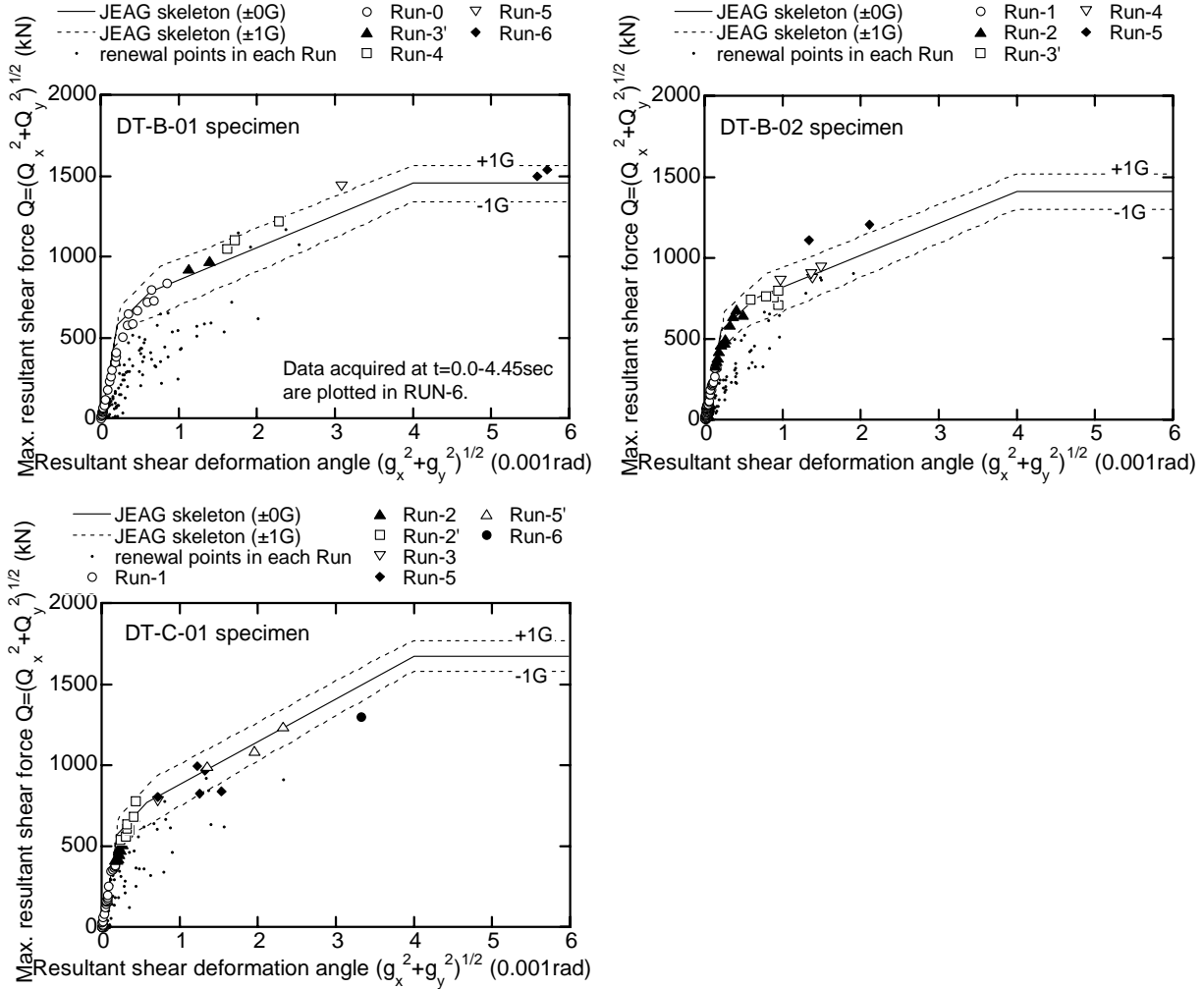


Fig.18 Renewal points of maximum resultant shear force plotted against resultant shear deformation angle and compared with evaluated skeleton curves for uni-axial loading

Estimation of equivalent viscous damping factor

Equivalent viscous damping factor heq is derived ordinarily from a hysteresis loop of load-deformation relationship in the manner described in the left of Fig.19(a). In case of multi-axial loading, shape of load-deformation curves is tangled too much to apply usual method. It is also true that the time to draw a loop in x-direction seldom coincides with the time to draw a loop in y-direction. So a simple method shown in Fig.19(a) is used for trial estimation of heq .

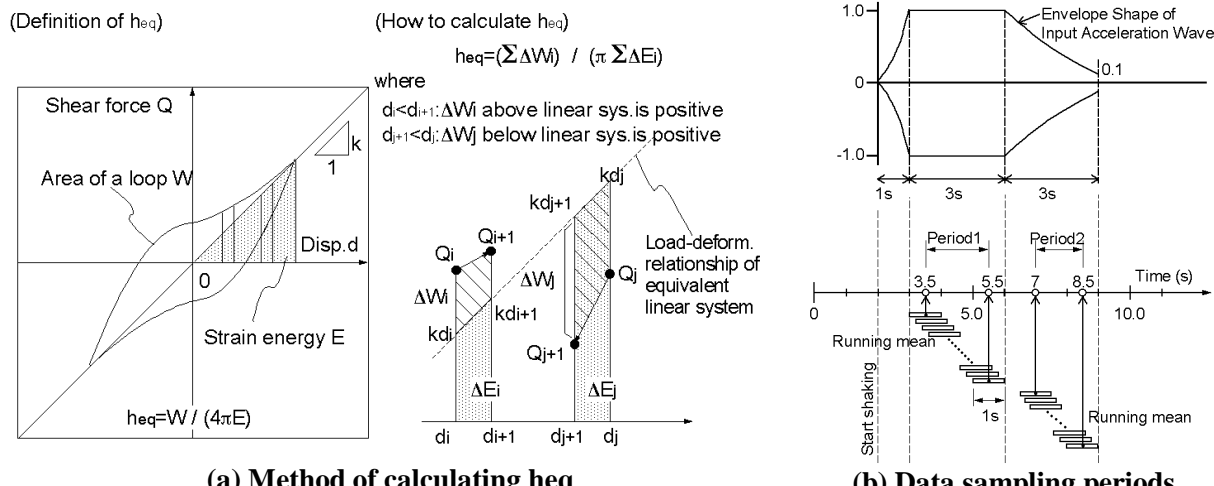
At first, a linear system is determined applying linear regression analysis to load-deformation relationship data like Fig.20. In this equivalent linear system, small increment of elastic strain energy between i-th and i+1-th data is defined as ΔE_i . The test data shows some deviation from the linear system in a sense of

energy. A small increment of the deviation is defined as ΔW_i . It is easy to calculate ΔE_i and ΔW_i at every moment. Equivalent viscous damping factor can be derived from sum of sufficient numbers of these small increments using equation in Fig.19(a).

The left graph of Fig.21 shows h_{eq} calculated by cumulation of ΔW_i and ΔE_i from the beginning of excitation. Damping factor h_{eq} tends to approach to some value as number of data increases. The right half of Fig.21 shows transition of h_{eq} derived by 1sec-running mean. The reason why h_{eq} decreases after $t=5.5$ sec seems to be in the envelope shape of the input excitation. Fig.22 - Fig.24 are h_{eq} by running mean calculated in period1 and period2 shown in Fig.19(b). X-axis is the maximum value of deformation angle among all data within a width of running mean. It seems that values of h_{eq} in the left graphs regarding period1 are higher than those in the right graphs regarding period2 because of plastic hysteresis damping due to strong excitation. This tendency is obvious in DT-B-02 and h_{eq} in period1 is about 0.02 higher than h_{eq} in period2.

As a trial, the same procedure as is written above is applied to the test results of uni-axial loading[4,5]. Acceleration time history of input motion for the specimen U-1 is shown in Fig.25(a). Duration time of input excitation in this test is not so long, and amplitude of acceleration is large in period4 shown in Fig.25(a). So in Run-3 and Run-4 of U-1, data in period4 are processed. In case of Run-5 of U-1, however, data in period3 are used because of the failure of the specimen. Fig.25(b) shows that h_{eq} of Run-5 of U-1 just before failure fairly coincides with h_{eq} of DT-B-02 in period2, which includes plastic hysteresis damping. As h_{eq} of Run-3 and Run-4 of U-1 is close to h_{eq} of DT-B-02 in period1, it seems that plastic deformation is not so dominant in these Run.

The equivalent viscous damping factor derived in period1 can be taken as the lower limit of the factor of total damping including plastic hysteresis damping. On the other hand, the h_{eq} value derived in period2 shows the upper limit of sum of factors of viscous damping and structural damping, because it may include small plastic hysteresis damping. It is necessary to study more test results to determine an appropriate value of damping factor for multi-axial loading case.



(a) Method of calculating h_{eq}

Fig.19 How to evaluate equivalent viscous damping factor h_{eq}

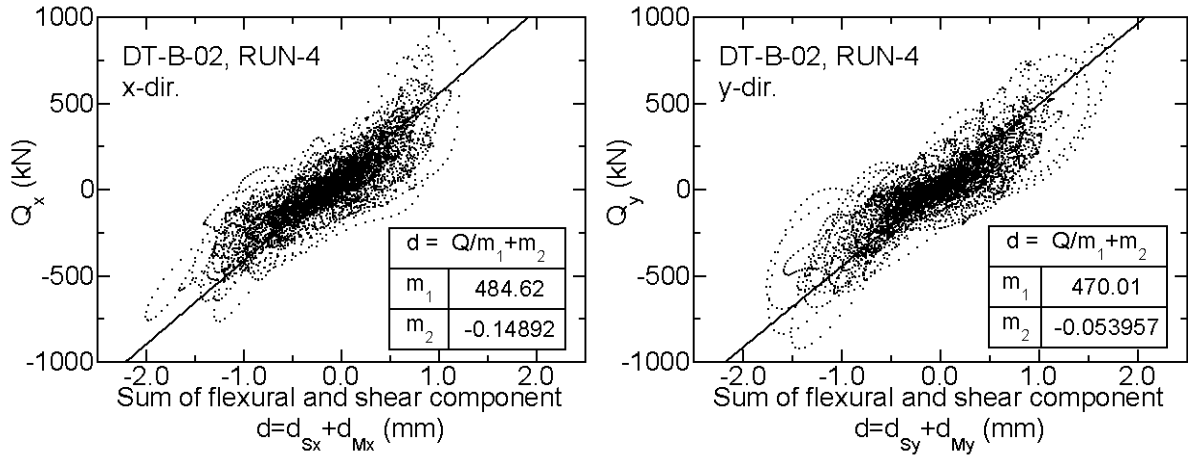


Fig.20 Linear regression to determine equivalent linear system

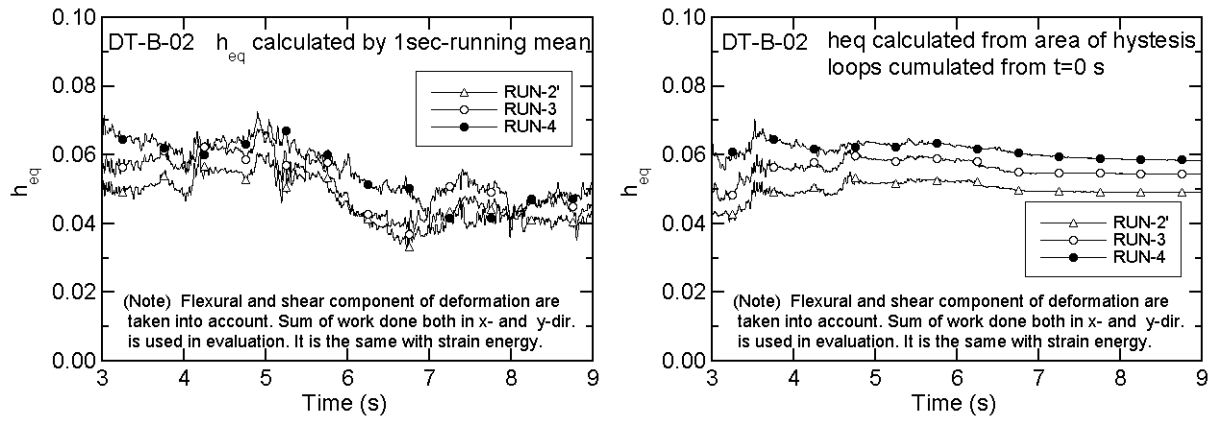


Fig.21 Transition of equivalent viscous damping factor

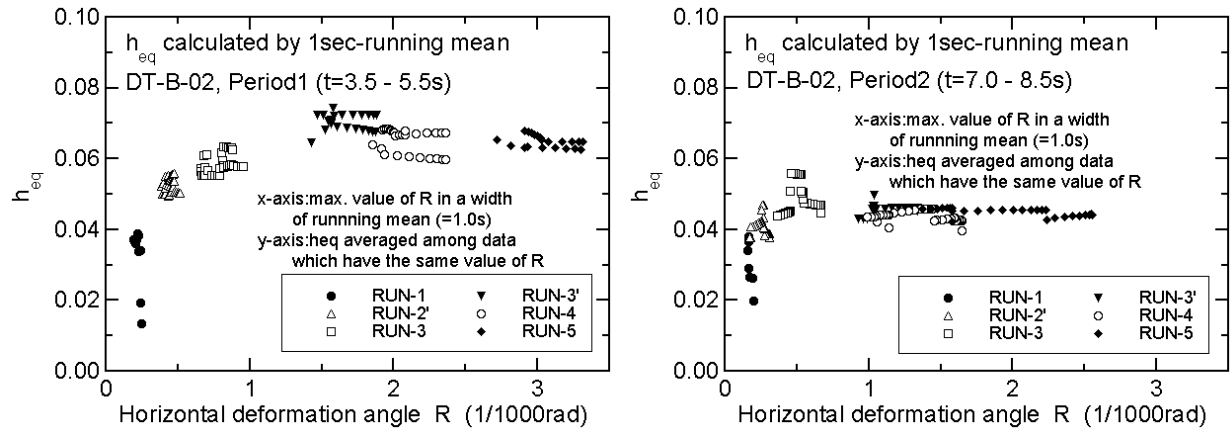


Fig.22 h_{eq} calculated by 1sec-running mean and related to max. deformation angle (DT-B-02)

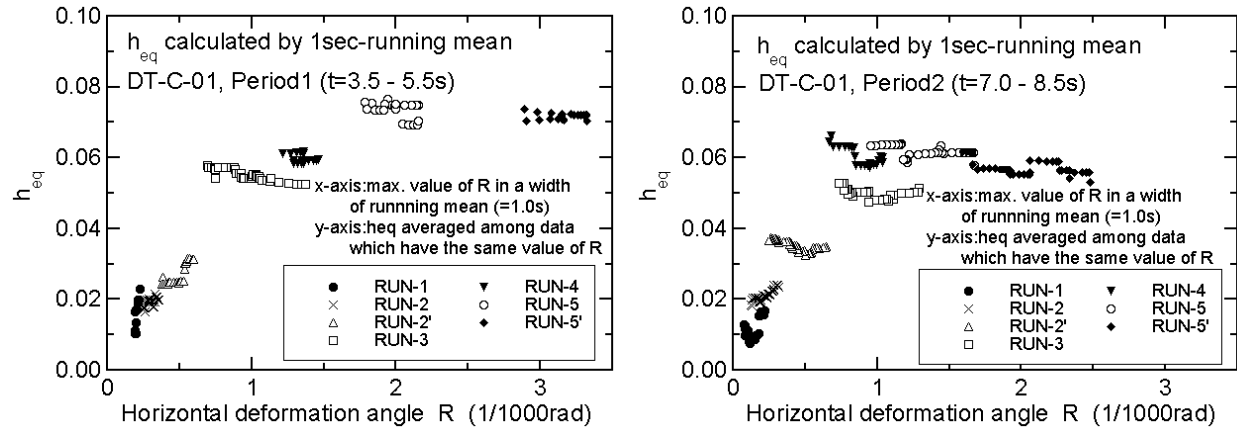


Fig.23 heq calculated by 1sec-running mean and related to max. deformation angle (DT-C-01)

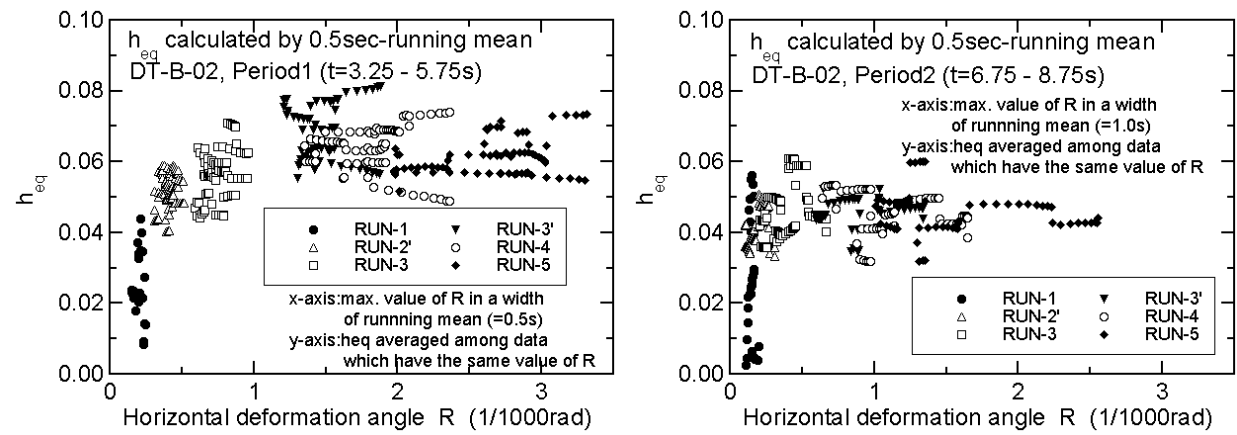
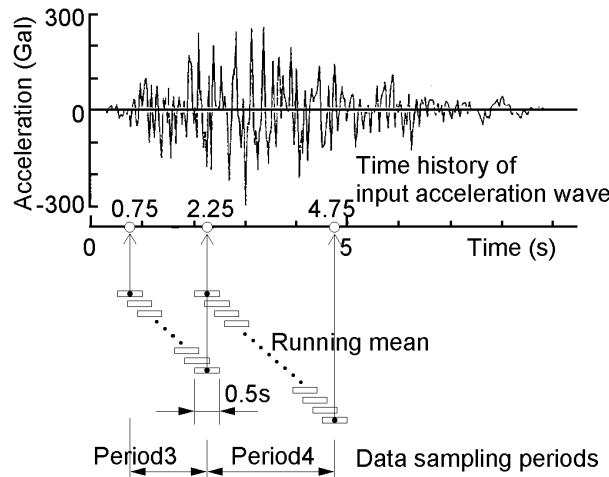
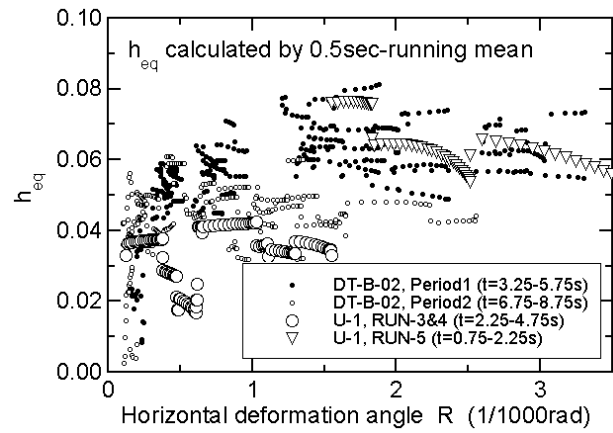


Fig.24 heq calculated by 0.5sec-running mean and related to max. deformation angle (DT-B-02)



(a) Input motion and data sampling periods

Fig.25 Equivalent viscous damping factor of uni-axial loading test[4,5]



(b) Comparison with results of DT-B-02

CONCLUDING REMARKS

Two box-type and one cylindrical RC shear wall specimens were tested using a tri-axial shaking table. Input motion of three independent components were applied to study fundamental response properties of RC seismic shear walls in wide range of responses from elastic region to an ultimate state.

With the test data, we discussed some characteristics of the RC seismic shear wall specimen. It is concluded that skeleton curve of shear force (Q) - shear deformation angle (γ) relationship derived from one directional static loading tests is effective, if horizontal response data are plotted on Q - γ plane as square root of sum of squares (SRSS) of response values in two directions. It is also concluded that values of equivalent viscous damping factor derived in trial estimation are close to those derived in one-directional loading tests.

The results can be used to evaluate engineering adequacies of the current design practice for RC shear walls of NPP structures. The test data is also available to improve seismic analysis codes for use in estimating a three-dimensional behavior of an RC building struck by a big earthquake ground motion.

ACKNOWLEDGEMENTS

Most part of this work was performed by NUPEC as a part of the "Model Test of Multi-axis Loading on RC Shear Walls" project commissioned by the Ministry of Economy, Trade and Industry (METI) of Japan. Technical issues have been discussed in the advisory committee on the project established by NUPEC (Chairperson: Professor Dr. Nishikawa). The authors wish to express many thanks to all the members of the committee for their valuable suggestions and co-operation.

REFERENCES

1. Survey Committee for Electro-technical Standard, Japan Electric Association, "Technical Guidelines for Aseismic Design of Nuclear Power Plants" (In Japanese), JEAG 4601-1987,1991, Japan Electric Association, Tokyo, JAPAN, 1987,1991.
2. Park,Y.J. and Hofmayer,C.H., "Technical Guidelines for Aseismic Design of Nuclear Power Plants, Translation of JEAG 4601-1987", NUREG/CR-6241, BNL-NUREG-52422, Brookheaven National Laboratory, Upton, N.Y., U.S.A., June 1994.
3. Ono,H., Maekawa,K. and Mitsugi,S., "The Influence of Vertical Input on the Horizontal Restoring Force Characteristics of Shear wall", Transactions of SMiRT17, Division H, #H03-4, Prague, August 2003.
4. OECD/NEA/CSNI, "SEISMIC SHEAR WALL ISP, NUPEC'S SEISMIC ULTIMATE DYNAMIC RESPONSE TEST, -Comparison Report-", NEA/CSNI/R(96)10, OECD/GD(96)188, 1996.
5. Kitada,Y., Akino,K., Terada,K., Aoyama,H. and Miller,A., "Report on seismic shear wall international standard problem organized by OECD/NEA/CSNI", Transactions of the 14th SMiRT, Vol5, pp.321-332.